

Exploring Intrinsic Magnetic Topological Insulators: The Case of EuIn_2As_2

Hao Liu,¹ Qi-Yi Wu,¹ Chen Zhang,¹ Jie Pang,^{2,3} Bo Chen,¹ Jiao-Jiao Song,¹ Yu-Xia Duan,¹ Ya-Hua Yuan,¹ Hai-Yun Liu,⁴ Chuan-Cun Shu,¹ Yuan-Feng Xu,⁵ You-Guo Shi,^{2,3} and Jian-Qiao Meng^{1,*}

¹*School of Physics, Central South University, Changsha 410083, Hunan, China*

²*Beijing National Laboratory for Condensed Matter Physics,*

Institute of Physics, Chinese Academy of Sciences, Beijing 100190, China

³*School of Physical Sciences, University of Chinese Academy of Sciences, Beijing 100049, China*

⁴*Beijing Academy of Quantum Information Sciences, Beijing 100085, China*

⁵*Center for Correlated Matter and School of Physics, Zhejiang University, Hangzhou 310058, China*

(Dated: Wednesday 6th November, 2024)

In this paper, ultrafast optical spectroscopy was employed to elucidate the intricate topological features of EuIn_2As_2 , a promising candidate for a magnetic topological crystalline axion insulator. Our investigation has revealed the exceptional sensitivity of the ultrafast carrier dynamics to the antiferromagnetic phase transition ($T_N \approx 16$ K). Below T_N , two distinct, extremely low-energy collective modes, ω_1 and ω_2 , with frequencies of ~ 9.9 and 21.6 GHz at $T = 4$ K, respectively, were observed, exhibiting strong temperature dependence. The higher-frequency mode is a magnon, and the lower-frequency mode, whose origin is currently uncertain, cannot be attributed to a coherent acoustic phonon. Additionally, high-fluence photoexcitation suggests the possibility of light-induced nonthermal phase transitions, such as the disruption of antiferromagnetic order. These findings provide insights into the interplay between topology and magnetism in EuIn_2As_2 , making it a promising candidate for applications in quantum information and spintronics.

I. INTRODUCTION

Topological insulators, a revolutionary class of quantum materials, manifest topological surface states within an insulating bulk [1, 2]. These surface states, protected by time-reversal symmetry (TRS), exhibit linear dispersion near Dirac points, rendering them impervious to non-magnetic perturbations. The introduction of additional magnetic order, disrupting TRS, results in magnetic topological materials with a unique band topology, promising distinct quantum phenomena [3, 4]. Recent theoretical predictions highlight EuIn_2As_2 as a compelling candidate [5], boasting intrinsic magnetic order and a three-dimensional hexagonal structure.

EuIn_2As_2 possesses a layered centrosymmetric crystal structure (space group $P6_3/mmc$, No. 194) with alternating stacking of Eu^{2+} and $[\text{In}_2\text{As}_2]^{2-}$ layers along the c axis, undergoing a paramagnetic (PM) to antiferromagnetic (AFM) transition at the Néel temperature $T_N \approx 16$ K [6, 7]. Theoretical frameworks propose EuIn_2As_2 as a potential topologically nontrivial magnetic insulator, capable of hosting AFM axion insulator phases [5, 8–10]. Advances in theoretical calculations underscore the critical influence of magnetic moment orientation on emergent topological states, predicting a topological crystalline insulator phase with some gapless surface states emerging on (100), (010), and (001) surfaces for in-plane oriented magnetic moments [5, 10, 11] and a higher-order topological insulator phase with gapped surface states emerging on (100) and (001) surfaces for out-of-plane oriented magnetic moments [5]. Unlike previously discovered material systems, density functional theory (DFT) calculations reveal that topological surface states in the stoichiometric form of EuIn_2As_2 are precisely located at the Fermi energy (E_F).

Despite progress in understanding, controversies persist, particularly regarding the nature of the axion-insulator phase,

such as whether there is a surface state energy gap associated with TRS breaking. Previous magnetic measurements indicate A -type AFM order in EuIn_2As_2 [6, 7], but recent neutron diffraction [8] and resonant elastic x-ray scattering [9] experiments suggest a low-symmetry helical AFM order, also satisfying the symmetry requirements for an axion insulator.

Magnetotransport measurements reveal negative magnetoresistance, indicating robust spin scattering by localized magnetic moments [6, 12]. Scanning tunneling microscopy and spectroscopy (STM/STS) data show a partial surface state gap (~ 40 meV) below T_N , diminishing with increasing temperatures but remaining finite above T_N [13]. Angle-resolved photoemission spectroscopy (ARPES) confirms hole-type Fermi pockets [10–12], a heavily hole-doped surface state, and inverted bulk bands in the AFM state [11], suggesting topological surface states are located above E_F . Notably, ARPES confirms the dominance of surface states near E_F , but fails to detect magnetic exchange gaps within them [10–12].

Ultrafast optical spectroscopy serves as a powerful tool for probing the intricate low-energy electron dynamics in correlated materials [14], offering insights into the complex behaviors of systems such as transition metal dichalcogenides [15, 16], high-temperature superconductors [17–21], and heavy fermions [22–25]. Sensitivity to changes in the low-energy electronic structure, especially the opening of narrow energy gaps near the E_F that may lead to bottleneck effects [17–26], renders it particularly valuable. Additionally, ultrafast optical spectroscopy excels in detecting collective bosonic excitations, providing a reliable indicator for phase transitions [22–24]. While ultrafast optical spectroscopy probes a material's bulk to a certain depth, it can offer valuable insights into the dynamics of surface states under specific conditions, particularly when surface states dominate the electronic structure near E_F , such as topological insulators [27, 28].

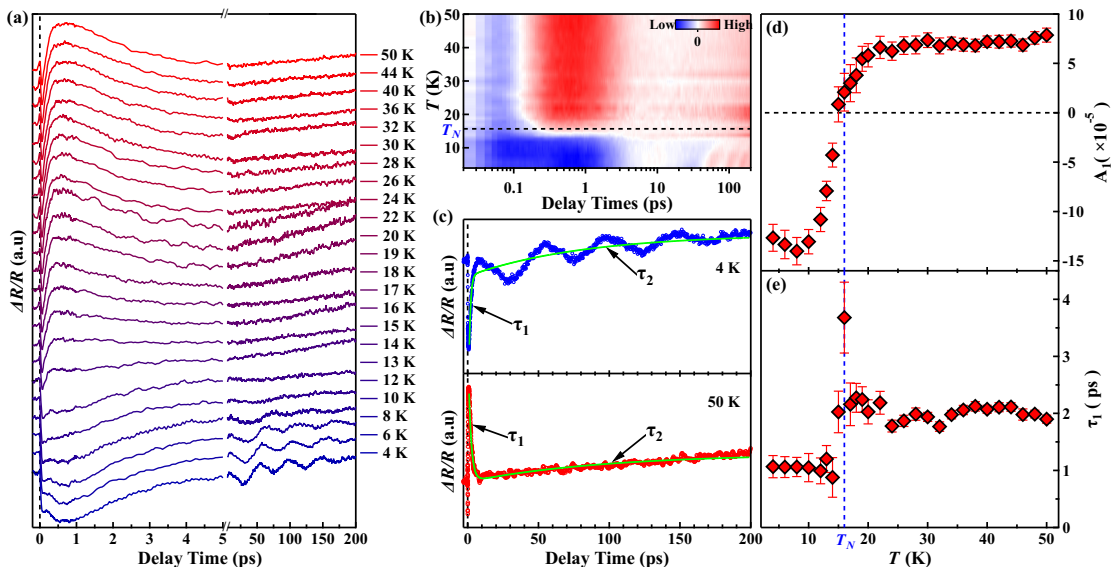


FIG. 1. (a) $\Delta R/R$ as a function of delay time over a temperature range from 4 to 50 K at a pump fluence of $53 \mu\text{J}/\text{cm}^2$. Note the break in the x axis. (b) Two-dimensional pseudocolor map of $\Delta R/R$ as a function of temperature and delay time. (c) Illustration of fitting using Eq. (1) (upper panel: 4 K; bottom panel: 50 K). The arrows indicate the corresponding relaxation process. (d) and (e) T dependence of A_1 and τ_1 , respectively.

Our study utilizes ultrafast optical spectroscopy to investigate the intricate topological states of EuIn_2As_2 , aiming to address current controversies and provide dynamic insights. Employing ultrafast techniques, we seek to unveil the real-time evolution of topological features, offering a nuanced understanding of the interplay between magnetism and topology in this fascinating material. The quasiparticle relaxation in EuIn_2As_2 undergoes a dramatic change in the vicinity of T_N . Below T_N , our measurements show the emergence of two extremely low-energy collective modes, ω_1 and ω_2 , with frequencies of ~ 9.9 and 21.6 GHz at $T = 4$ K, respectively, both exhibiting a strong temperature dependence. The temperature- and fluence-dependent measurements suggest that the origin of ω_1 remains unclear and cannot be attributed to a coherent acoustic phonon, while ω_2 is associated with a magnon. Moreover, our high-fluence photoexcitation results suggest the potential for photoinduced nonthermal phase transitions. Our findings firmly establish EuIn_2As_2 as a promising material for investigating the interplay between topology and magnetism.

II. EXPERIMENTAL DETAILS

High-quality single crystals of EuIn_2As_2 were grown utilizing the self-flux method [29], demonstrating a T_N of approximately 16 K (refer to Fig. S1 in the Supplemental Material for the magnetic measurements [30]). We performed ultrafast time-resolved differential reflectivity measurements ($\Delta R/R$) at a center wavelength of 800 nm (~ 1.55 eV) using a 1 MHz Yb-based femtosecond (fs) laser oscillator [17]. These measurements were carried out on a freshly cleaved (001) surface under a high vacuum of 10^{-6} mbar. The pump and probe

beams were focused on the sample at nearly normal incidence, with spot diameters of approximately $85 \mu\text{m}$ for the pump beam and $40 \mu\text{m}$ for the probe beam. The pump and probe beams were s and p polarized, respectively.

III. RESULTS AND DISCUSSIONS

Figure 1(a) presents the differential reflectivity $\Delta R/R$ of EuIn_2As_2 at various temperatures (4-50 K) at a pump fluence of $\sim 53 \mu\text{J}/\text{cm}^2$. Photoexcitation induces immediate changes in $\Delta R/R$, followed by multiple recovery processes with different lifetimes, indicating diverse relaxation pathways. The curves exhibit a pronounced temperature dependence. Notably, the peak around 0.7 ps transforms into a valley with decreasing temperature. Below T_N , damped oscillations appear after a few picoseconds. These observations contrast with the minimal temperature dependence reported by Wu *et al.* [36]. The discrepancy likely stems from the different pump wavelengths (800 nm vs. 400 nm). Above T_N , optical conductivity suggests a transition from the valence to the conduction band at a wave number corresponding to 800 nm. Below T_N , the AFM transition splits the valence band [35]. Therefore, transient reflectivity using an 800 nm pump wavelength offers a more sensitive probe of the AFM transition in EuIn_2As_2 compared to the approach employed by Wu *et al.* [36].

Figure 1(b) presents a two-dimensional (2D) map of $\Delta R/R$ (pump-probe delay versus temperature). The initial relaxation (~ 0.3 ps) reveals pronounced variations in $\Delta R/R$ near T_N , with a clear positive-to-negative signal transition. This behavior confirms $\Delta R/R$ effectiveness in capturing electronic structure changes during the AFM transition. It aligns with expectations [22] and supports prior findings from ARPES [10, 11]

and infrared spectroscopy [35] of significant alterations in the electronic structure during the AFM transition.

A quantitative analysis of quasiparticle dynamics was conducted to investigate its temperature-dependent behavior. We focus here on recombination processes occurring after electron-electron and electron-phonon thermalization, when carriers have already relaxed to the vicinity of the E_F [37]. The solid green lines in Fig. 1(c) suggests that the nonoscillatory response over a considerable time domain (~ 1 -200 ps) fits well with a bi-exponential decay, using the expression

$$\frac{R(t)}{R} = \sum_{i=1,2} A_i \exp\left(-\frac{t-t_0}{\tau_i}\right) + C \quad (1)$$

where A_i is the amplitude and τ_i is the relaxation time of the i th nonoscillatory signal which describes carrier dynamics. C is a constant representing long-lifetime processes.

Figures 1(d) and 1(e) show the temperature dependence of extracted amplitude (A_1) and relaxation time (τ_1). Both exhibit anomalies near T_N , reflecting the influence of AFM order on electron-hole recombination [38]. A_1 displays a slow decrease followed by a rapid drop and sign reversal near T_N before saturating at lower temperatures. Similarly, the relaxation time τ_1 exhibits a sharp change around T_N . These behaviors, reminiscent of those observed in superconductors [17–21] and heavy fermion compounds [22–25], have been attributed to the opening of a narrow energy gap in the density of states (DOS) near E_F . STM/STS measurements [13] and DFT calculations [8, 10] show that the spin-orbit coupling-induced bulk gap varies little across T_N and persists above it. Furthermore, theoretical studies suggest that the AFM transition may open a gap at the Dirac cone of the surface state, regardless of whether the AFM order is out of plane [5, 10] or helical [8]. Notably, the sign inversion of A_1 near T_N introduces significant uncertainties in the fitting process for A_1 and τ_1 . Therefore, our data are insufficient to conclusively support the existence of this gap. Thus, we attribute the anomalies in both A_1 and τ_1 to changes in the bulk electronic structure [35], rather than the opening of a narrow bulk or surface magnetic gap. Future work using time-resolved and angle-resolved photoemission spectroscopy (TR-ARPES) will be crucial to precisely characterize the unoccupied band structure, particularly its temperature dependence and the gap position relative to E_F .

Following the low-fluence analysis, we investigated low-frequency collective bosonic excitations, known indicators of phase transitions [22, 23, 39]. Figure 2(a) depicts time-domain oscillations extracted from the low-temperature transient reflectivity data [Fig. 1(a)] after background removal. The oscillation periods and amplitudes vary with temperature, increasing and decreasing, respectively. Notably, the oscillations are exclusively observed below T_N and vanish above it.

Oscillatory components were extracted by performing fast Fourier transform (FFT). Figure 2(b) presents two pronounced extremely low-energy modes, ω_1 and ω_2 , at frequencies of ~ 9.9 (i.e., 0.04 meV or 0.33 cm^{-1}) and ~ 21.6 GHz (i.e., 0.09

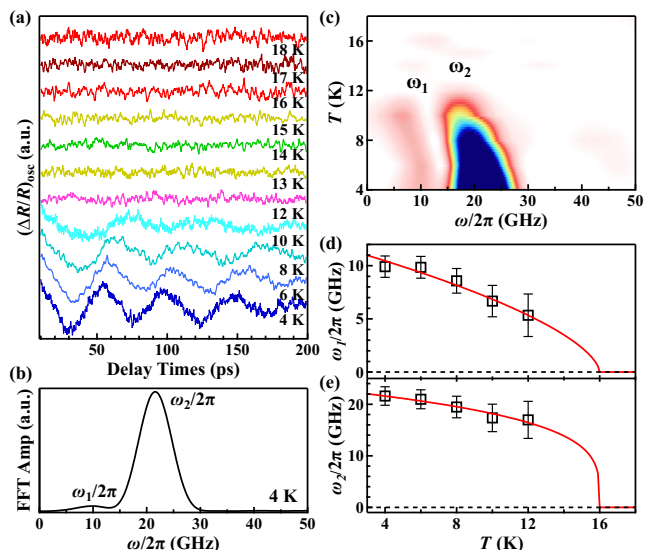


FIG. 2. (a) Extracted oscillations over a temperature range from 4 to 18 K at a pump fluence of $53 \mu\text{J}/\text{cm}^2$. Curves are shifted for clarity. (b) Fast Fourier transform (FFT) frequency-domain data at 4 K. (c) FFT spectrum color intensity map as a function of frequency and temperature. (d) and (e) The derived frequencies of ω_1 and ω_2 as a function of temperature. The red lines are fits described in the main text.

meV or 0.71 cm^{-1}) at a temperature of 4 K. Figure 2(c) displays the FFT spectrum as a function of frequency and temperature. The two gigahertz modes, ω_1 and ω_2 , were exclusively observed at temperatures lower than T_N , with both frequencies consistently diminishing and experiencing softening as T_N is approached. The presence of the two extremely low-energy modes is limited to temperatures below T_N , suggesting they are either of magnetic origin or highly responsive to the magnetic ordering.

The extracted temperature dependence of ω_1 and ω_2 frequencies is plotted in Figs. 2(d) and 2(e), respectively. The temperature dependence of ω_1 and ω_2 can be effectively fitted using a mean-field-like T dependence [40], $\omega = \omega(0)(1 - T/T_N)^{2\beta}$, where $T_N = 16$ K and β are the Néel temperature and critical exponent, respectively. This fitting yields zero-temperature frequencies of $\omega_1(0) \simeq 12.5$ GHz and $\omega_2(0) \simeq 23.2$ GHz, with corresponding β values of $\beta_{\omega_1} \simeq 0.31$ and $\beta_{\omega_2} \simeq 0.123$, respectively. $2\beta_{\omega_2}$ matches the expected value of 0.25 for a two-dimensional Ising system [41]. These results are consistent with the magnetic susceptibility measurements, suggesting that EuIn_2As_2 is a two-dimensional antiferromagnet [7, 12]. This noteworthy observation unequivocally confirms the intrinsically 2D character of EuIn_2As_2 's magnetic ordering, which has been observed in other antiferromagnets, such as the two-dimensional antiferromagnet NiPS_3 [42]. At a pump fluence of $180 \mu\text{J}/\text{cm}^2$, Wu *et al.*'s time-resolved magneto-optical Kerr effect (TR-MOKE) measurements have revealed an 18 GHz spin precession mode under low magnetic fields, disappearing above T_N , while a persistent 35 GHz coherent acoustic phonon mode persists up to 25 K in

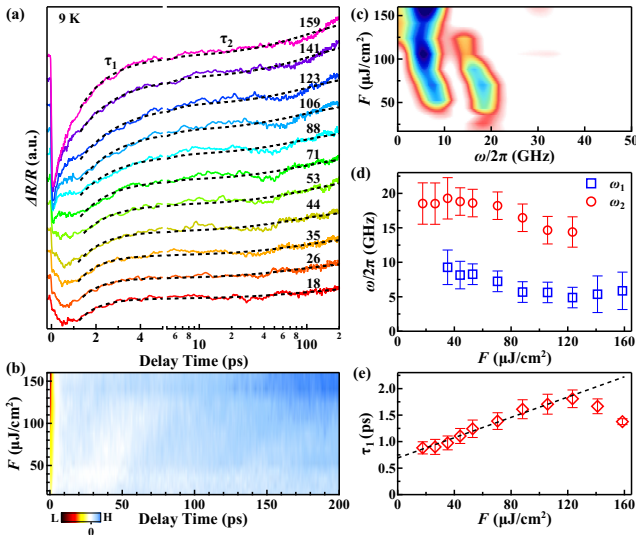


FIG. 3. (a) Fluence dependence of the $\Delta R/R$ as a function of delay time at 9 K over a long time scales. The black solid lines are Eq. (1) fits. (b) 2D pseudocolor map of $\Delta R/R$ as a function of delay time over a fluence range from 18 to 159 $\mu\text{J}/\text{cm}^2$. (c) FFT spectrum color intensity map as a function of frequency and fluence. (d) The derived frequencies of ω_1 and ω_2 as a function of fluence. (e) Fluence dependence of τ_1 . The black dashed line represents the linear fit to the low fluence data.

high magnetic fields [36].

Considering that our measurements were conducted without the influence of a magnetic field, and given that the ω_2 mode disappears after a magnetic phase transition induced by intense pump fluence (to be discussed in detail later), we infer that the ω_2 mode originates from magnetic order, signifying its nature as a magnon. The localized Eu $4f$ spin, positioned approximately 1.7 eV below E_F and energetically separated from the initial optical excitation (1.55 eV), is effectively probed by ultrafast optical spectroscopy due to its strong interatomic exchange coupling with bulk topological bands. In EuIn_2As_2 , below T_N , electrons excited from In $5s$ and As $4p$ orbitals decay to the ground state via two primary mechanisms: electron-phonon coupling-induced spin flips and spin-orbit coupling-induced spin flips. Consequently, the localized Eu $4f$ spins undergo disorder through coupling with spin-flipped sp orbital electrons, leading to coherent magnon emission to conserve angular momentum. This process, akin to impulsive stimulated Raman scattering (ISRS) via spin-flip scattering, resembles an ultrafast inverse Cotton-Mouton effect, where the linearly polarized excitation pulse acts on spins as a short effective field pulse [42–44]. Ultrafast optical spectroscopy functions as a powerful tool for characterizing nonequilibrium spin dynamics and their intricate interplay with electrons and the lattice. The temperature evolution of the lower-frequency oscillation ω_1 differs, exhibiting distinct critical parameters compared to ω_2 . However, with the above dataset, we are unable to ascertain the origin of ω_1 .

In light of the complex magnetic structure revealed by low-

temperature magnetization and magnetotransport measurements in EuIn_2As_2 [12], indicating the potential for an external field-induced phase transition, we conducted a fluence-dependent measurement at 9 K [Fig. 3(a)] to explore the characteristics of two modes and investigate potential photon-induced transient phase transitions. The $\Delta R/R$ response exhibits notable variations, with the well-defined reflectivity valley structure around 0.7 ps progressively suppressed and disappearing under high fluence (beyond 123 $\mu\text{J}/\text{cm}^2$). The simplification of the reflectivity curve’s lineshape implies the closure of specific relaxation channels as pump fluence surpasses the threshold. Figure 3(b) presents a 2D pseudocolor map of $\Delta R/R$ as a function of pump-probe delay (x -axis) and fluence (y -axis). The map reveals clear long-period oscillations that exhibit fluence-dependent behavior. For a detailed analysis of oscillations and quasiparticle relaxation, we applied Eq. (1) to fit the fluence-dependent transient reflectivity beyond ~ 1 ps, achieving a good fit, as illustrated by the black dashed lines in Fig. 3(a).

FFT was utilized to extract the oscillations, and Fig. 3(c) presents the FFT spectrum in terms of frequency and fluence. Notably, ω_1 is challenging to discern at low fluence, while ω_2 becomes indiscernible at high fluence. The derived frequencies of ω_1 and ω_2 , displayed in Fig. 3(d), offer further insights. For fluences below ~ 71 $\mu\text{J}/\text{cm}^2$, ω_2 remains nearly constant, subtly softening at higher fluence, and becoming undetectable beyond 123 $\mu\text{J}/\text{cm}^2$. In contrast, ω_1 , initially indiscernible at low fluence, exhibits gradual softening and even slight abnormal hardening beyond 123 $\mu\text{J}/\text{cm}^2$. In addition, Fig. 3(c) shows that the FFT amplitude of the ω_1 mode increases with the rise in pump fluence. The derived τ_1 was plotted in Fig. 3(e) as a function of pump fluence. Initially, τ_1 increases almost monotonically linearly with fluence, but beyond 123 $\mu\text{J}/\text{cm}^2$, it decreases with further fluence, aligning partially with observations in MnBi_4Te_7 , where an increase in relaxation time with fluence was reported [38]. Calculations suggest that ω_1 could not be a coherent acoustic phonon induced by thermal stress (see details in the Supplemental Material [30]). Therefore, we consider that the ω_1 mode might be excited by acoustic waves through a laser-induced magnetoelastic mechanism [45, 46]. However, further experiments and theoretical models are required to determine the origin of ω_1 .

To address the reduced τ_1 and the anomalous behavior of two modes beyond 123 $\mu\text{J}/\text{cm}^2$, we considered two possibilities: firstly, intense pumping causing pronounced heating, elevating the temperature of the illuminated area. Despite the lack of direct low-temperature thermal conductivity measurements [47], a preliminary estimation at 9 K was conducted for EuIn_2As_2 . The observed lower resistivity in EuIn_2As_2 [6, 7, 12] compared to its newly formed layered compound, $\beta\text{-EuIn}_2\text{As}_2$ [48], along with the higher specific heat in EuIn_2As_2 [7] than in $\beta\text{-EuIn}_2\text{As}_2$ [48], suggests that the thermal conductivity of EuIn_2As_2 possibly exceeds that of $\beta\text{-EuIn}_2\text{As}_2$ [48]. Consequently, at 9 K, the estimated thermal conductivity of EuIn_2As_2 is approximately 40 W/m·K. This

estimation aligns with various measurements [6, 7, 10–12], including ARPES [10–12], supporting the characterization of EuIn_2As_2 as a metal. Considering optical constants [35] and a worst-case scenario (base temperature of 9 K and excitation density of $159 \mu\text{J}/\text{cm}^2$), a sample steady-state heat diffusion model [21] suggests that the average laser-induced heating in EuIn_2As_2 is less than 0.8° and can be neglected. Second, we consider a photon-inducing rapid nonthermal phase transition, such as the quenching of magnetic order [21, 22, 49]. High fluence likely disrupts the long-range AFM order, leading to a light-induced transient magnetic phase transition, accompanied by specific relaxation channels. Future work should focus on verifying these transitions using TR-ARPES to better understand the ultrafast changes in the band structure, as well as direct measurements of magnetic order under ultrafast photoexcitation. These studies would provide further insights into the possibility of controlling AFM order and the potential for creating transient magnetic phases in EuIn_2As_2 .

IV. CONCLUSIONS

In summary, our ultrafast optical spectroscopy study of EuIn_2As_2 has provided critical insights into its antiferromagnetic phase transition and the interplay between magnetism and topology. We observed a dramatic change in quasiparticle relaxation dynamics around the Néel temperature ($T_N \approx 16$ K), along with the emergence of two distinct low-energy collective modes ω_1 (~ 9.9 GHz) and ω_2 (~ 21.6 GHz) below T_N . Although the origin of the ω_1 mode is currently unknown and cannot be attributed to a coherent acoustic phonon, the ω_2 mode is associated with a magnon, and both exhibit strong temperature dependence, highlighting the intricate coupling between magnetic order and the material's electronic structure. Moreover, high-fluence photoexcitation experiments suggest the possibility of light-induced nonthermal phase transitions, such as the quenching of antiferromagnetic order. This indicates the potential for manipulating magnetic phases in EuIn_2As_2 using ultrafast laser pulses, opening new avenues for exploring dynamic magnetic phenomena. Our results establish EuIn_2As_2 as a promising platform for studying the interplay between magnetism and topology, with potential applications in quantum information and spintronics. Further investigations, particularly using techniques such as time-resolved and angle-resolved photoemission spectroscopy, will be crucial for precisely characterizing these phase transitions and their implications for topological surface states. These future studies may unlock different opportunities for controlling magnetic order and realizing transient magnetic phases in magnetic topological materials.

ACKNOWLEDGMENTS

This work was supported by National Key Research and Development Program of China (Grant No. 2022YFA1604204), the National Natural Science Foundation of China (Grants No. 12074436, U2032204, U22A6005, and 12374163), the Science and Technology Innovation

Program of Hunan province (Grant No. 2022RC3068), the Strategic Priority Research Program of the Chinese Academy of Sciences (Grant No. XDB33010000), the Changsha Natural Science Foundation (Grant No. kq2208254), and the Fundamental Research Funds for the Central Universities of Central South University (Grant No. 1053320215412). We are grateful for resources from the High Performance Computing Center of Central South University.

* Corresponding author: jqmeng@csu.edu.cn

- [1] M. Z. Hasan and C. L. Kane, Colloquium: Topological insulators, *Rev. Mod. Phys.* **82**, 3045 (2010).
- [2] X. L. Qi and S. C. Zhang, Topological insulators and superconductors, *Rev. Mod. Phys.* **83**, 1057 (2011).
- [3] B. A. Bernevig, C. Felser, and H. Beidenkopf, Progress and prospects in magnetic topological materials, *Nature* **603**, 41 (2022).
- [4] Y. F. Xu, L. Elcoro, Z. Song, B. J. Wieder, M. G. Vergniory, N. Regnault, Y. Chen, C. Felser, and B. A. Bernevig, High-throughput calculations of magnetic topological materials, *Nature* **586**, 702 (2020).
- [5] Y. F. Xu, Z. Song, Z. Wang, H. Weng, and X. Dai, Higher-Order Topology of the Axion Insulator EuIn_2As_2 , *Phys. Rev. Lett.* **122**, 256402 (2019).
- [6] A. M. Goforth, P. Klavins, J. C. Fettinger, and S. M. Kazalari, Magnetic Properties and Negative Colossal Magnetoresistance of the Rare Earth Zintl phase EuIn_2As_2 , *Inorg. Chem.* **47**, 11048 (2008).
- [7] P. F. S. Rosa, C. Adriano, T. M. Garitezi, R. A. Ribeiro, Z. Fisk, and P. G. Pagliuso, Electron spin resonance of the intermetallic antiferromagnet EuIn_2As_2 , *Phys. Rev. B* **86**, 094408 (2012).
- [8] S. X. M. Riberolles, T. V. Trevisan, B. Kuthanazhi, T. W. Heitmann, F. Ye, D. C. Johnston, S. L. Bud Ko, D. H. Ryan, P. C. Canfield, A. Kreyssig, A. Vishwanath, R. J. McQueeney, L. L. Wang, P. P. Orth, and B. G. Ueland, Magnetic crystalline-symmetry-protected axion electrodynamics and field-tunable unpinned Dirac cones in EuIn_2As_2 , *Nat. Commun.* **12**, 999 (2021).
- [9] J. Soh, A. Bombardi, F. Mila, M. C. Rahn, D. Prabhakaran, S. Francoual, H. M. Rønnow, and A. T. Boothroyd, Understanding unconventional magnetic order in a candidate axion insulator by resonant elastic x-ray scattering, *Nat. Commun.* **14**, 3387 (2023).
- [10] S. Regmi, M. M. Hosen, B. Ghosh, B. Singh, G. Dhakal, C. Sims, B. Wang, F. Kabir, K. Dimitri, Y. Liu, A. Agarwal, H. Lin, D. Kaczorowski, A. Bansil, and M. Neupane, Temperature-dependent electronic structure in a higher-order topological insulator candidate EuIn_2As_2 , *Phys. Rev. B* **102**, 165153 (2020).
- [11] T. Sato, Z. Wang, D. Takane, S. Souma, C. Cui, Y. Li, K. Nakayama, T. Kawakami, Y. Kubota, C. Cacho, T.K. Kim, A. Arab, V.N. Strocov, Y. Yao, and T. Takahashi, Signature of band inversion in the antiferromagnetic phase of axion insulator candidate EuIn_2As_2 , *Phys. Rev. Res.* **2**, 033342 (2020).
- [12] Y. Zhang, K. Deng, X. Zhang, M. Wang, Y. Wang, C. Liu, J. W. Mei, S. Kumar, E.F. Schwier, K. Shimada, C. Y. Chen, and B. Shen, In-plane antiferromagnetic moments and magnetic polaron in the axion topological insulator candidate EuIn_2As_2 , *Phys. Rev. B* **101**, 205126 (2020).

- [13] M. Gong, D. Sar, J. Friedman, D. Kaczorowski, S. Abdel Razeq, W. C. Lee, and P. Aynajian, Surface state evolution induced by magnetic order in axion insulator candidate EuIn_2As_2 , *Phys. Rev. B* **106**, 125156 (2022).
- [14] D. N. Basov, R. D. Averitt, D. van der Marel, M. Dressel, and K. Haule, Electrodynamics of correlated electron materials, *Rev. Mod. Phys.* **83**, 471 (2011).
- [15] S. X. Zhu, C. Zhang, Q. Y. Wu, X. F. Tang, H. Liu, Z. T. Liu, Y. Luo, J. J. Song, F. Y. Wu, Y. Z. Zhao, S. Y. Liu, T. Le, X. Lu, H. Ma, K. H. Liu, Y. H. Yuan, H. Huang, J. He, H. Y. Liu, Y. X. Duan, and J. Q. Meng, Temperature evolution of quasiparticle dispersion and dynamics in semimetallic 17-TiTe_2 via high-resolution angle-resolved photoemission spectroscopy and ultrafast optical pump-probe spectroscopy, *Phys. Rev. B* **103**, 115108 (2021).
- [16] J. Qi, X. Chen, W. Yu, P. Cadden-Zimansky, D. Smirnov, N. H. Tolk, I. Miotkowski, H. Cao, Y. P. Chen, Y. Wu, S. Qiao, and Z. Jiang, Ultrafast carrier and phonon dynamics in Bi_2Se_3 crystals, *Appl. Phys. Lett.* **97**, 182102 (2010).
- [17] C. Zhang, Q. Y. Wu, W. S. Hong, H. Liu, S. X. Zhu, J. J. Song, Y. Z. Zhao, F. Y. Wu, Z. T. Liu, S. Y. Liu, Y. H. Yuan, H. Huang, J. He, S. L. Li, H. Y. Liu, Y. X. Duan, H. Q. Luo, and J. Q. Meng, Ultrafast optical spectroscopy evidence of pseudogap and electron-phonon coupling in an iron-based superconductor $\text{KCa}_2\text{Fe}_4\text{As}_4\text{F}_2$, *Sci. China-Phys. Mech. Astron.* **65**, 237411 (2022).
- [18] Q. Y. Wu, C. Zhang, Z. Z. Li, W. S. Hong, H. Liu, J. J. Song, Y. Z. Zhao, Y. H. Yuan, B. Chen, X. Q. Ye, S. L. Li, J. He, H. Y. Liu, Y. X. Duan, H. Q. Luo, and J. Q. Meng, Hidden nematic fluctuation in the triclinic $(\text{Ca}_{0.85}\text{La}_{0.15})_{10}(\text{Pt}_3\text{As}_8)(\text{Fe}_2\text{As}_2)_5$ superconductor revealed by ultrafast optical spectroscopy, *Phys. Rev. B* **108**, 205136 (2023).
- [19] Q. Y. Wu and J. Q. Meng, Ultrafast optical spectroscopy of FeAs-based superconductors, *Sci. Sin.: Phys. Mech. Astron.* **53**, 127408 (2023).
- [20] V. V. Kabanov, J. Demsar, B. Podobnik, and D. Mihailovic, Quasiparticle relaxation dynamics in superconductors with different gap structures: Theory and experiments on $\text{YBa}_2\text{Cu}_3\text{O}_{7-\delta}$, *Phys. Rev. B* **59**, 1497 (1999).
- [21] J. Demsar, J. L. Sarrao, and A. J. Taylor, Dynamics of photoexcited quasiparticles in heavy electron compounds, *J. Phys.: Condens. Matter* **18**, R281 (2006).
- [22] Y. Z. Zhao, Q. Y. Wu, C. Zhang, B. Chen, W. Xia, J. J. Song, Y. H. Yuan, H. Liu, F. Y. Wu, X. Q. Ye, H. Y. Zhang, H. Huang, H. Y. Liu, Y. X. Duan, Y. F. Guo, J. He, and J. Q. Meng, Coupling of optical phonons with Kondo effect and magnetic order in the antiferromagnetic Kondo-lattice compound CeAuSb_2 , *Phys. Rev. B* **108**, 075115 (2023).
- [23] K. S. Burch, E. E. M. Chia, D. Talbayev, B. C. Sales, D. Mandrus, A. J. Taylor, and R. D. Averitt, Coupling between an Optical Phonon and the Kondo Effect, *Phys. Rev. Lett.* **100**, 026409 (2008).
- [24] Y. P. Liu, Y. J. Zhang, J. J. Dong, H. Lee, Z. X. Wei, W. L. Zhang, C. Y. Chen, H. Q. Yuan, Y. F. Yang, and J. Qi, Hybridization Dynamics in CeCoIn_5 Revealed by Ultrafast Optical Spectroscopy, *Phys. Rev. Lett.* **124**, 057404 (2020).
- [25] J. Qi, T. Durakiewicz, S. A. Trugman, J. X. Zhu, P. S. Riseborough, R. Baumbach, E. D. Bauer, K. Gofryk, J. Q. Meng, J. J. Joyce, A. J. Taylor, and R. P. Prasankumar, Measurement of Two Low-Temperature Energy Gaps in the Electronic Structure of Antiferromagnetic USb_2 Using Ultrafast Optical Spectroscopy, *Phys. Rev. Lett.* **111**, 057402 (2013).
- [26] A. Rothwarf and B. N. Taylor, Measurement of Recombination Lifetimes in Superconductors, *Phys. Rev. Lett.* **19**, 27 (1967).
- [27] V. Iyer, Y. P. Chen, and X. F. Xu, Ultrafast Surface State Spin-Carrier Dynamics in the Topological Insulator $\text{Bi}_2\text{Te}_2\text{Se}$, *Phys. Rev. Lett.* **121**, 026807 (2018).
- [28] P. Sharma, A. Bhardwaj, R. Sharma, V. P. S. Awana, T. N. Narayanan, K. V. Raman, and M. Kumar, Comprehensive Study of the topological Surface States through Ultrafast Pump-probe Spectroscopy, *J. Phys. Chem. C* **126**, 11138(2022).
- [29] Y. Li, H. Deng, C. Wang, S. Li, L. Liu, C. Zhu, K. Jia, Y. Sun, X. Du, X. Yu, T. Guan, R. Wu, S. Zhang, Y. Shi, and H. Mao, Surface and electronic structure of antiferromagnetic axion insulator candidate EuIn_2As_2 , *Acta Phys. Sin.* **70**, 186801 (2021).
- [30] See Supplemental Material at **** for additional experimental results and a supporting data analysis, which includes Refs.[12, 31–36].
- [31] D. Lim, R. D. Averitt, J. Demsar, A. J. Taylor, N. Hur, and S. W. Cheong, Coherent acoustic phonons in hexagonal manganite LuMnO_3 , *Appl. Phys. Lett.* **83**, 4800 (2003).
- [32] M. Takahara, H. Jinn, S. Wakabayashi, T. Moriyasu, and T. Kohmoto, Observation of coherent acoustic phonons and magnons in an antiferromagnet NiO , *Phys. Rev. B* **86**, 094301 (2012).
- [33] D. Wang, A. Cross, G. Guarino, S. Wu, R. Sobolewski, and A. Mycielski, Time-resolved dynamics of coherent acoustic phonons in CdMnTe diluted-magnetic single crystals, *Appl. Phys. Lett.* **90**, 211905 (2007).
- [34] F. H. Yu, H. M. Mu, W. Z. Zhuo, Z. Y. Wang, Z. F. Wang, J. J. Ying, and X. H. Chen, Elevating the magnetic exchange coupling in the compressed antiferromagnetic axion insulator candidate EuIn_2As_2 , *Phys. Rev. B* **102**, 180404(R) (2020).
- [35] B. Xu, P. Marsik, S. Sarkar, F. Lyzwa, Y. Zhang, B. Shen, and C. Bernhard, Infrared study of the interplay of charge, spin, and lattice excitations in the magnetic topological insulator EuIn_2As_2 , *Phys. Rev. B* **103**, 245101 (2021).
- [36] Q. Wu, T. Hu, D. Wu, R. Li, L. Yue, S. Zhang, S. Xu, Q. Liu, T. Dong, and N. Wang, Spin dynamics in the axion insulator candidate EuIn_2As_2 , *Phys. Rev. B* **107**, 174411 (2023).
- [37] H. Li, S. Y. Gao, S. F. Duan, Y. F. Xu, K. J. Zhu, S. J. Tian, J. C. Gao, W. H. Fan, Z. C. Rao, J. R. Huang, J. J. Li, D. Y. Yan, Z. T. Liu, W. L. Liu, Y. B. Huang, Y. L. Li, Y. Liu, G. B. Zhang, P. Zhang, T. Kondo, S. Shin, H. C. Lei, Y. G. Shi, W. T. Zhang, H. M. Weng, T. Qian, and H. Ding, Dirac Surface States in Intrinsic Magnetic Topological Insulators EuSn_2As_2 and $\text{MnBi}_{2n}\text{Te}_{3n+1}$, *Phys. Rev. X* **9**, 041039 (2019).
- [38] P. E. Majchrzak, Y. Liu, K. Volckaert, D. Biswas, C. Sahoo, D. Puntel, W. Bronsch, M. Tuniz, F. Cilento, X. Pan, Q. Liu, Y. P. Chen, and S. Ulstrup, van der Waals engineering of ultrafast carrier dynamics in magnetic heterostructures, *Nano Lett.* **23**, 414 (2023).
- [39] Y. S. Wang, B. Chen, Z. T. Liu, X. Guo, S. You, Z. Wang, H. Xie, T. Niu, J. Q. Meng, and H. Huang, In-plane electron-phonon coupling anisotropy and multiple charge density wave orders in the superconductor $\text{Bi}_2\text{Rh}_3\text{Se}_2$, *Phys. Rev. B* **108**, 045118 (2023).
- [40] R. V. Yusupov, T. Mertelj, J. H. Chu, I. R. Fisher, and D. Mihailovic, Single-Particle and Collective Mode Couplings Associated with 1- and 2-Directional Electronic Ordering in Metallic $R\text{Te}_3$ ($R = \text{Ho}, \text{Dy}, \text{Tb}$), *Phys. Rev. Lett.* **101**, 246402 (2008).
- [41] M. F. Collins, *Magnetic Critical Scattering* (Oxford University Press, Oxford, U.K., 1989).
- [42] D. Afanasiev, J. R. Hortensius, M. Matthesen, S. Mañas-Valero, M. Šiškins, M. Lee, E. Lesne, H. S. J. van der Zant, P. G. Steeneken, B. A. Ivanov, E. Coronado, and A. D. Caviglia, Controlling the anisotropy of a van der Waals antiferromagnet with light, *Sci. Adv.* **7**, eabf3096 (2021).

- [43] A. M. Kalashnikova, A. V. Kimel, R. V. Pisarev, V. N. Gridnev, A. Kirilyuk, and T. Rasing, Impulsive Generation of Coherent Magnons by Linearly Polarized Light in the Easy-Plane Antiferromagnet FeBO_3 , *Phys. Rev. Lett.* **99**, 167205 (2007).
- [44] J. Nishitani, T. Nagashima, and M. Hangyo, Terahertz radiation from antiferromagnetic MnO excited by optical laser pulses, *Appl. Phys. Lett.* **103**, 081907 (2013).
- [45] T. Parpiiev, A. Hillion, V. Vlasov, V. Gusev, K. Dumesnil, T. Hauet, S. Andrieu, A. Anane, and T. Pezeril, Ultrafast strain excitation in highly magnetostrictive terfenol: Experiments and theory, *Phys. Rev. B* **104**, 224426 (2021).
- [46] Y. Shin, M. Vomir, D. Kim, P. C. Van, J. Jeong, and J. Kim, Quasi-static strain governing ultrafast spin dynamics, *Communications Physics* **5**, 56 (2022).
- [47] K. Shinozaki, Y. Goto, K. Hoshi, R. Kiyama, N. Nakamura, A. Miura, C. Moriyoshi, Y. Kuroiwa, H. Usui, and Y. Mizuguchi, Thermoelectric Properties of the As/P-Based Zintl Compounds $\text{EuIn}_2\text{As}_{2-x}\text{P}_x$ ($x = 0-2$) and SrSn_2As_2 , *ACS Appl. Energy Mater.* **4**, 5155 (2021).
- [48] D. S. Wu, S. H. Na, Y. J. Li, X. B. Zhou, W. Wu, Y. T. Song, P. Zheng, Z. Li, and J. L. Luo, Single-crystal growth, structure and thermal transport properties of the metallic antiferromagnet Zintl-phase β - EuIn_2As_2 , *Phys. Chem. Chem. Phys.* **26**, 8695 (2024).
- [49] V. A. Stoica, D. Puggioni, J. Zhang, R. Singla, G. L. Dakovski, G. Coslovich, M. H. Seaberg, M. Kareev, S. Middey, P. Kissin, R. D. Averitt, J. Chakhalian, H. Wen, J. M. Rondinelli, and J. W. Freeland, Magnetic order driven ultrafast phase transition in NdNiO_3 , *Phys. Rev. B* **106**, 165104 (2022).